

DRAFT VERSION APRIL 16, 2024
Typeset using L^AT_EX preprint2 style in AASTeX62

Multipolar Electromagnetic Emission of Newborn Magnetar

YU WANG,^{1,2,3} RAHIM MORADI,⁴ AND LIANG LI^{1,2,3}

¹*ICRA and Dipartimento di Fisica, Sapienza Università di Roma, P.le Aldo Moro 5, 00185 Rome, Italy.*

²*ICRANet, P.zza della Repubblica 10, 65122 Pescara, Italy.*

³*INAF – Osservatorio Astronomico d’Abruzzo, Via M. Maggini snc, I-64100, Teramo, Italy.*

⁴*Key Laboratory of Particle Astrophysics, Institute of High Energy Physics, Chinese Academy of Sciences, Beijing 100049, China.*

ABSTRACT

It is generally recognized that the electromagnetic multipolar emission from magnetars can be used to explain radiation from Soft Gamma Repeaters (SGRs) or Anomalous X-ray Pulsars (AXPs), but they have little impact on the spindown of magnetars. We here present a comprehensive analytical solution for the neutron star multipolar electromagnetic fields and their associated expected luminosities. We find that for newborn millisecond magnetars, the spin-down luminosity from higher multipolar components can match or even exceed that from the dipole component. Such high-intensity radiation will undoubtedly affect related astrophysical phenomena at the birth of a magnetar. We show that the spin-down luminosity from multipoles can well explain the majority of Gamma-Ray Bursts (GRBs) afterglows, from the plateau starting at several hundred seconds till the normal decay phase lasting for many years. The fitted magnetar parameters for GRB afterglows are all typical values, with spins in the millisecond range and magnetic field strengths in the order of $10^{14} - 10^{15}$ Gauss. Our results in turn, provide support for the hypothesis that GRBs originate from the birth of magnetars with a few millisecond period, thus deepening our understanding of the complex magnetic field structure and the equation of state of magnetars.

1. INTRODUCTION

Our understanding of neutron stars (NSs) is largely derived from phenomena related to its magnetic fields (Lattimer & Prakash 2004, 2007;

Kaspi 2010; Igoshev et al. 2021b). Since, apart from the rare gravitational wave observations (Abbott et al. 2017a), the low-frequency radio and high-energy X-ray pulses, as well as the higher-energy transitional flares, are all related to their strong magnetic fields, which generate electromagnetic radiation either by accelerating charged particles or through its own dissipation (Meszaros 1992; Lyne & Graham-Smith 2005; Esposito et al. 2021).

Corresponding author: Rahim Moradi, Yu Wang,
Liang Li

rmoradi@ihep.ac.cn

yu.wang@inaf.it

liang.li@icranet.org

Research on the magnetic fields of NSs has historically focused on the dipole component for two primary reasons: First, the dipole model has a simple mathematical form, of which the first-order approximation sufficiently accounts for the majority of observational data (Gunn & Ostriker 1969; Michel 1982). Indeed, the inaugural observation of the NS in 1968 could be explained by magnetic dipole radiation (Hewish et al. 1968; Ostriker & Gunn 1969). Second, the strength of higher-order multipoles decreases more rapidly than that of the dipole with distance from the NS. Consequently, the dipole normally dominates the radiation at large distances. Most of our observations of NSs, such as the spin-down rate and the pulsar wind geometry, are of far-field radiation, which can be effectively explained by dipole radiation. Detecting the signatures of higher-order multipoles emanating from small-size regions which require high-resolution observations is challenging (Kundt & Schaaf 1993; Philippov & Kramer 2022).

Thanks to the refinement of theoretical models, increased complexity of computer simulations, and continuous development of observational techniques, studies are increasingly integrating multipolar components to explain and predict the complex behaviors observed in NSs, particularly in strongly magnetized NS known as magnetars (Turolla et al. 2015; Kaspi & Beloborodov 2017; Papitto et al. 2020; Igoshev et al. 2021b; Philippov & Kramer 2022; Taverna & Turolla 2024).

Theoretically, multipole fields near the surface are generally required to facilitate the production of electron-positron pairs in the magnetosphere (Ruderman & Sutherland 1975). And the theory that the polar cap is anchored with a multiple field (Gil et al. 2006) is supported by the discovery that the area heated by X-ray is significantly smaller than traditional polar cap size (Zhang et al. 2005). Observationally, SGR

0418+5729 presents a typical case. Its complex and strong multipolar fields, of strength as high as 10^{15} Gauss measured by the proton cyclotron lines (Tiengo et al. 2013), produce the observed X-ray bursts (Rea et al. 2010; Turolla et al. 2011). While its spindown reveal a dipolar magnetic field of only $B_p \simeq 6 \times 10^{12}$ G (Rea et al. 2013). The multipole components can also channel energy and heat to localized areas on the surface of NSs, creating hot spots (Huang & Yu 2014; Geppert & Viganò 2014; Riley et al. 2019; de Lima et al. 2020; Kalapotharakos et al. 2021; De Grandis et al. 2021). The detection of thermal X-ray pulsations from the hot surface of PSR J0030+0451 by the NS Interior Composition Explorer (NICER) telescope suggests that pulsars are originated from the global-scale multipolar magnetic fields (Bilous et al. 2019). In addition, multipoles are required in explaining the observations of flare activities, irregular timing properties, detailed X-ray analysis, and etc (see e.g. Scholz et al. 2014; Turolla et al. 2015; Igoshev et al. 2021a; Wang et al. 2021; Suvorov 2023; Fiori et al. 2024).

The examples provided above primarily focus on multipolar radiation characteristics occurring at least a century after the formation of the NS. However, to comprehensively understand the formation of magnetars, the complex magnetic structure, the equation of state, and their evolution, observations from hundreds of years later are insufficient. Early-stage information is needed to gain a more complete understanding. But as of now, early information is not sufficiently discovered. The Chandra Deep Field-South survey (CDF-S) has provided the sole recognized early-stage observation, capturing the X-ray transient known as CDF-S XT2, a magnetar just born from the binary NS merger (Xue et al. 2019).

To obtain early information about magnetars, our approach is to examine multipolar radiation, particularly starting from the moment of

their formation. Magnetars can theoretically form from binary NS mergers and from single star collapse. The formation of magnetar is associated with and plays a critical role in various areas of astrophysics, including superluminous supernova (SLSNs), gamma-ray bursts (GRBs) and fast radio bursts (FRBs).

SLSNe are supernovae that are approximately 100 times more luminous than typical supernovae. Some SLSNe are believed to be powered by newly formed magnetars, with the rotational energy being converted into electromagnetic radiation, enhancing the brightness of the supernova explosion (Woosley 2010; Kasen & Bildsten 2010). FRBs are brief, intense extragalactic radio flashes, and one hypothesis suggests they could be related to magnetars, either through the magnetars' own activities or processes associated with their formation (Petroff et al. 2022; Zhang 2023). GRBs are intense flashes of gamma-rays that can last from a fraction of a second to several minutes, followed by an X-ray afterglow that persists for years (Piran 2004; Berger 2014). In this paper we will specifically focus on GRBs to highlight the significance of newborn magnetars in astrophysical events.

This article is structured to flow logically, beginning with Section 2 and 3, where we discuss magnetar emissions: we examine the theoretical model of multipolar emission from a newborn magnetar and present the expected luminosity lightcurve by demonstrating some cases. Following this, Section 4 offers a concise overview of phenomena related to magnetars, with a special focus on GRB. In Section 5, we apply the magnetar multipolar model to the afterglow observations of GRBs, uncovering a consistency between the predicted magnetar evolution and the observed plateau and subsequent normal decay phases of GRB afterglows. Finally, Section 6 delves into our findings, examining their limitations and broader implications.

2. MODELING MULTIPOLAR SPIN-DOWN AND EMISSION

The electromagnetic field of NS is described by the Maxwell equations with the boundary conditions, the equations can be decomposed then solved by introducing a set of vector spherical harmonics (Jackson 1998; Barrera et al. 1985). Each harmonic mode is identified by a set of multipole order number l and azimuthal mode number m . Therefore, we have the magnetic multipoles, including dipole ($l = 1$), quadrupole ($l = 2$), hexapole ($l = 3$), octopole ($l = 4$) and higher orders. Considering a rotating NS in a vacuum, Pétri (2015) gives a complete analytical solution of the NS multipolar electromagnetic fields, which is adopted in this article. For simplicity, instead of considering the finite size of the NS, we take the simplified solution treating NS as a point-like source.

Magnetic dipole is the lowest multipolar component, which has been well studied and is considered as the only magnetic field in the majority GRB articles concerning the energy injection from a NS or a magnetar (for e.g. Dai & Lu 1998; Zhang & Mészáros 2001; Turolla et al. 2015; Li et al. 2018; Liang et al. 2007). The spin-down energy loss rate (luminosity) by Poynting flux is

$$L_{\text{dip}} = \frac{2}{3c^3} \Omega^4 B_{\text{dip}}^2 R^6 \Theta_{\text{dip}}^2 \quad (1)$$

$$\Theta_{\text{dip}}^2 = \sin^2 \chi_1 \quad (2)$$

where Ω is the angular velocity of the NS, B_{dip} is the dipole magnetic field strength, R is the radius of the NS, c is the speed of light, Θ_{dip} contains the angle-related terms, χ_1 is the inclination angles of the magnetic dipole moment, related to the azimuthal mode number m , $\chi_1 = 0$ or 90 degrees for $m = 0$ or 1 . The rotational energy of the NS E_{rot} evolve as

$$\frac{dE_{\text{rot}}}{dt} = I\Omega\dot{\Omega} = -L \quad (3)$$

where I is the momentum of inertia and L is the energy loss rate. For a pure dipole $L = L_{\text{dip}}$, the above equation gives the solution of the evolution of the angular velocity

$$\Omega = \Omega_0 \left(1 + \frac{t}{\tau_{\text{dip}}}\right)^{-1/2}, \quad (4)$$

and the energy loss rate

$$L_{\text{dip}} = L_{\text{dip},0} \left(1 + \frac{t}{\tau_{\text{dip}}}\right)^{-2} \quad (5)$$

where Ω_0 is initial angular velocity, τ_{dip} characterizes the time scale of the NS losing half of its rotational energy

$$\tau_{\text{dip}} = \frac{3Ic^3}{4\Omega_0^2 B_{\text{dip}}^2 R^6 \Theta_{\text{dip}}^2} \quad (6)$$

and $L_{\text{dip},0}$ is the initial energy loss rate

$$L_{\text{dip},0} = \frac{I\Omega_0^2}{2\tau_{\text{dip}}} \quad (7)$$

The angular velocity Ω decreases slowly before τ_{dip} , then follows almost a power-law decay with index $-1/2$. Correspondingly, the energy loss rate L_{dip} keeps almost a constant before τ_{dip} , then drops with power-law index -2 , since the dipole energy loss $L_{\text{dip}} \propto \Omega^4$. The characteristic timescale τ_{dip} relates to all the properties of the NS, a more massive, slower spin, lower magnetic field, smaller radius NS corresponds to a longer τ_{dip} . The initial energy loss rate $L_{\text{dip},0}$ is simply in the form of the total rotational energy $I\Omega_0^2/2$ divided by the characteristic timescale τ_{dip} .

Magnetic quadrupole can be easily generated, for example, the north pole and the south pole of the magnetic axis are not aligned in a line. Given a quadrupole magnetic field B_{quad} , the energy loss rate is

$$L_{\text{quad}} = \frac{32}{135c^5} \Omega^6 B_{\text{quad}}^2 R^8 \Theta_{\text{quad}}^2, \quad (8)$$

$$\Theta_{\text{quad}}^2 = \sin^2 \chi_1 (\cos^2 \chi_2 + 10 \sin^2 \chi_2) \quad (9)$$

where the angular term Θ_{quad} contains two inclination angles, χ_1 reminisces the dipole field, χ_2 relates to the quadrupole field, the different choice of $\chi_2 = 0$ or 90 degrees brings a factor of 10 difference. For a pure magnetic quadrupole, $L = L_{\text{quad}}$, equation 3 gives the evolution of the spin

$$\Omega = \Omega_0 \left(1 + \frac{t}{\tau_{\text{quad}}}\right)^{-1/4}, \quad (10)$$

and the loss rate of the rotational energy

$$L_{\text{quad}} = L_{\text{quad},0} \left(1 + \frac{t}{\tau_{\text{quad}}}\right)^{-3/2} \quad (11)$$

where the characteristic timescale of quadrupole emission

$$\tau_{\text{quad}} = \frac{135Ic^5}{128\Omega_0^4 B_{\text{quad}}^2 R^8 \Theta_{\text{quad}}^2} \quad (12)$$

and the initial energy loss rate

$$L_{\text{quad},0} = \frac{I\Omega_0^2}{4\tau_{\text{quad}}} \quad (13)$$

Compared to the dipole field, the energy loss rate of quadrupole field is more sensitive to the spin of the NS, since $L_{\text{quad}} \propto \Omega^6$ and $L_{\text{dip}} \propto \Omega^4$. Consequently, the energy loss rate L_{quad} at time later than the characteristic timescale τ_{quad} follows a shallower power-law decay than the dipole field, with power-law index $-3/2$.

Magnetic hexapole, octopole and higher-order poles are from high-order harmonic modes. The spin-down luminosities of hexapole and octopole are

$$L_{\text{hexa}} = \frac{2}{4725\pi c^7} \Omega^8 B_{\text{hexa}}^2 R^{10} \Theta_{\text{hexa}}^2 \quad (14)$$

and

$$L_{\text{octo}} = \frac{4}{297675\pi c^9} \Omega^{10} B_{\text{octo}}^2 R^{12} \Theta_{\text{octo}}^2, \quad (15)$$

respectively. The related angular terms are more complicated, for hexapole field,

$$\Theta_{\text{hexa}}^2 = \sin^2 \chi_1 (29 \cos^2 \chi_2 + \sin^2 \chi_2 (1664 \cos^2 \chi_3 + 15309 \sin^2 \chi_3)), \quad (16)$$

an additional inclination angle χ_3 is involved, $\Theta_{\text{hexa}}^2 = \{29, 1664, 15309\}$ for the configurations of $\{\chi_1, \chi_2, \chi_3\} = \{(90, 0, 0), (90, 90, 0), (90, 90, 90)\}$ degrees. The octopole field has one more angle χ_4 ,

$$\Theta_{\text{octo}}^2 = \sin^2 \chi_1 (23 \cos^2 \chi_2 + \sin^2 \chi_2 (5632 \cos^2 \chi_3 + \sin^2 \chi_3 (133407 \cos^2 \chi_4 + 1179648 \sin^2 \chi_4))), \quad (17)$$

which gives $\Theta_{\text{octo}}^2 = \{23, 5632, 133407, 1179648\}$ for the configuration of $\{\chi_1, \chi_2, \chi_3, \chi_4\} = \{(90, 0, 0, 0), (90, 90, 0, 0), (90, 90, 90, 0), (90, 90, 90, 90)\}$ degrees.

For a pure hexapole, the spin and the luminosity change as

$$\Omega = \Omega_0 \left(1 + \frac{t}{\tau_{\text{hexa}}}\right)^{-1/6}, \quad (18)$$

$$L_{\text{hexa}} = L_{\text{hexa},0} \left(1 + \frac{t}{\tau_{\text{hexa}}}\right)^{-4/3} \quad (19)$$

where the characteristic timescale and the initial luminosity are

$$\tau_{\text{hexa}} = \frac{4725\pi I c^7}{12\Omega_0^6 B_{\text{hexa}}^2 R^{10} \Theta_{\text{hexa}}^2} \quad (20)$$

$$L_{\text{hexa},0} = \frac{I\Omega_0^2}{6\tau_{\text{hexa}}} \quad (21)$$

For the energy loss by a pure octopole, the spin and the luminosity decreases as

$$\Omega = \Omega_0 \left(1 + \frac{t}{\tau_{\text{octa}}}\right)^{-1/8}, \quad (22)$$

$$L_{\text{octa}} = L_{\text{octa},0} \left(1 + \frac{t}{\tau_{\text{octa}}}\right)^{-5/4} \quad (23)$$

where the characteristic timescale and the initial luminosity are

$$\tau_{\text{octa}} = \frac{297675\pi I c^9}{32\Omega_0^8 B_{\text{octa}}^2 R^{12} \Theta_{\text{octa}}^2} \quad (24)$$

$$L_{\text{octa},0} = \frac{I\Omega_0^2}{8\tau_{\text{octa}}} \quad (25)$$

Generally, for multipole with order number l , the luminosity is in the form of

$$L_l = C_l \Omega^{2l+2} B_l^2 R^{2l+4} \Theta_l^2 \quad (26)$$

where C_l is a constant, B_l is the magnetic field, Θ_l is the angular term. The time evolution of the angular velocity and the luminosity are

$$\Omega = \Omega_0 \left(1 + \frac{t}{\tau_l}\right)^{-2l}, \quad (27)$$

$$L_{\text{hexa}} = L_{l,0} \left(1 + \frac{t}{\tau_l}\right)^{-1-1/l}. \quad (28)$$

The characteristic timescale and initial luminosity are

$$\tau_l = \frac{I c^{2l+1}}{(2l+2) C_l \Omega_0^{2l} B_l^2 R^{2l+4} \Theta_l^2} \quad (29)$$

$$L_{l,0} = \frac{I\Omega_0^2}{2l\tau_l} \quad (30)$$

3. MULTIPOLAR LUMINOSITY EVOLUTION

The magnetic field structure of magnetar is an issue that is continuously being explored (Igoshev et al. 2021b). Based on current theories and observations, it is generally recognized that the magnetic field structure is very complex. Besides the large-scale dipolar poloidal field, there can also exist other scales of multipolar poloidal fields and toroidal fields.

Toroidal fields influence the spin-down rate by affecting the internal dynamics of the star and its interaction with the surrounding environment. This is an indirect and extremely complex process (Gourgouliatos & Hollerbach 2018). Therefore, this article, aiming to provide a first-order approximate picture, does not consider the toroidal fields.

Regarding the relationship between the dipole and high-order multipoles, it lacks a consensus. First, the formation of magnetic field of magnetars remains a topic of extensive discussion. There are numerous processes proposed to augment and reconfigure the magnetic

field during the proto-NS phase (Igoshev et al. 2021b). Taking the classical dynamo model as an example, there could be an orderly dynamo that generates a strong dipole field, or it could be a stochastic dynamo, which generates strong multipolar fields with a weak dipolar field (Thompson & Duncan 1993; Gourgouliatos et al. 2016; Igoshev et al. 2021b). Secondly, the observed magnetic field strengths of magnetars exhibit a wide range. Most magnetars¹ (Olausen & Kaspi 2014), identified by SGRs or AXPs, have their dipolar magnetic field strengths calculated to exceed the quantum critical field strength, $B_Q \approx 4.4 \times 10^{13}$ Gauss. These calculations are based on the observed spin periods and spin-down rates, employing the dipole model. However, there are magnetars with dipolar field below the quantum critical field B_Q , such as SGR 0418+5729 (Rea et al. 2010), Swift J1822.3-1606 (Rea et al. 2012), and 3XMM J185246.6+003317 (Rea et al. 2014). Among these, SGR 0418+5729 has a lowest dipolar field as $B_p \simeq 6 \times 10^{12}$ Gauss (Rea et al. 2013). The question of whether these lower-strength dipolar magnetic fields are inherently low at the time of formation or have decayed from higher intensities remains under discussion (Alpar et al. 2011; Turolla et al. 2011; Turolla & Esposito 2013). Theoretical models suggest that the high-order multipoles could be even stronger than the dipole, possibly reaching values up to several times 10^{15} Gauss (Gourgouliatos et al. 2016). Observationally, determining the strength of higher-order multipolar is complex, largely because these components mainly influence only the localized phenomena. Their existence and strengths are often inferred from, such as, the distribution of surface hotspots, the details of the emission spectra, and the energetics of flares and outbursts. For instance,

although SGR 0418+5729 does not meet the typical magnetar standard in terms of dipole field strength, the observation of cyclotron absorption features implies the existence of a complex magnetic field, with strengths reaching 10^{15} Gauss near the surface (Tiengo et al. 2013). The SGR J1935+2154, associated with FRBs (Kirsten et al. 2021), has a dipolar magnetic field strength of 4.4×10^{14} Gauss, obtained from changes in its spin period, aligning with typical magnetar values. Further analysis of fitting its X-ray spectra with the STEMS3D model, reveals a stronger, local nondipolar magnetic field of 9.6×10^{14} Gauss (Gögüş et al. 2020).

Summarizing the above, magnetars can exhibit both dipole and high-order multipole magnetic field components. The dipole field strength may either exceed or fall below the critical field threshold, while the multipole fields are consistently above it. The strength of the multipole field surpasses that of the dipole field in any individual magnetar. This pattern holds true at least for the currently observed limited number of samples.

These confirmed magnetars are relatively young compared to normal NSs, with ages ranging from a few thousand to tens of thousands of years, magnetars with weaker dipole fields may be older (Mereghetti et al. 2015; Mondal 2021). Inferring the initial strength of the magnetic field from observations made thousands of years later is not straightforward, as different theoretical models yield varying results (Igoshev et al. 2021b). Generally, magnetic fields decay over time, but it is also possible for initially buried magnetic fields to emerge, leading to an increase in field strength (Geppert et al. 1999).

In light of the aforementioned considerations, we present three scenarios to visualize the evolution of the quiescent luminosity starting from the birth of the magnetars using the formulae derived in section 2. We use typical values and

¹ McGill Online Magnetar Catalog: <http://www.physics.mcgill.ca/~pulsar/magnetar/main.html>

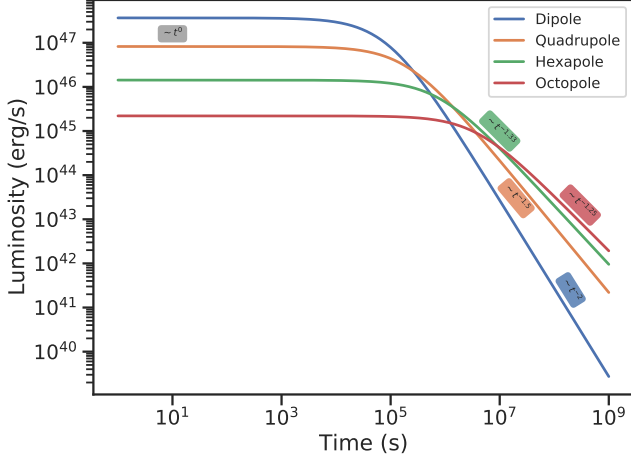


Figure 1. The spin-down luminosity of different multipoles with the same magnetic strength ($B = 10^{14}$ G), respectively. All show a plateau phase, followed by a power-law-like decay, the higher order multipole produces a shallower decay.

do not account for the evolution of the magnetic fields.

The first scenario involves that only one magnetic field component exists, or one component overwhelmingly dominates. We examine the radiation evolution of dipole, quadrupole, hexapole, and octopole independently. By setting the magnetic field strength of 10^{14} Gauss, selecting the maximum values of the angular factors of different multipoles as $\Theta_{\text{dip}}^2 = 1$, $\Theta_{\text{quad}}^2 = 10$, $\Theta_{\text{hexa}}^2 = 15338$, $\Theta_{\text{octo}}^2 = 1179671$, along with the initial spin of 1 ms, the radius of 1.2×10^6 cm and the mass of $1.4M_{\odot}$ (the same angular factors, initial spin, radius, and mass values will be applied in subsequent examples), we generate figure 1. It can be observed that both dipoles and multipoles feature an initial plateau phase followed by a power-law decay phase. The plateau phase luminosity is highest for the dipole, with the luminosity of multipoles proportionally decreasing as the order increases. Correspondingly, the characteristic age proportionally increases. The power-law index in the decay phase is steepest for the dipole at -2, with the quadrupole, hexapole, and octopole respectively at -1.5, -1.33, and -1.25.

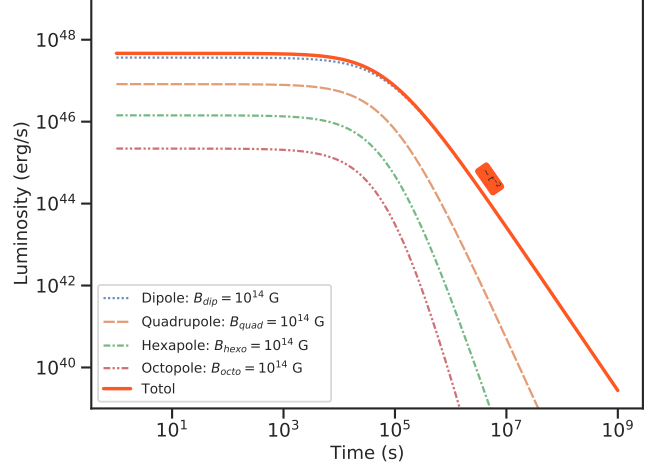


Figure 2. A magnetar having dipole, quadrupole, hexapole and octopole, of which the strength of magnetic fields are the same ($B = 10^{14}$ G). The dipole dominates the evolution all the time.

It is important to note that most observed magnetars, having evolved over thousands of years, have spin periods on the order of seconds, whereas we are considering newly born magnetars with millisecond-level spins. The spindown luminosity of higher-order multipoles is more sensitive to the spin period. On the order of seconds spin, the multipole spindown luminosity is negligible compared to the dipole. This supports our previous discussion that the dipole determines the spindown rate, while multipoles only affect near-field phenomena. However, for newly born magnetars with milliseconds spins, the spindown luminosities from adjacent multipolar orders does not differ by orders of magnitudes. Our subsequent examples even demonstrate that under certain magnetic field configurations, multipoles can produce a brighter spindown luminosity than the dipole.

The second scenario involves the simultaneous existence of the dipole, quadrupole, hexapole, and octopole, with all magnetic field strengths set at 10^{14} Gauss. The results, as shown in figure 2, indicate that the dipole dominates the spindown throughout the entire period. The contribution of the multipoles gradually de-

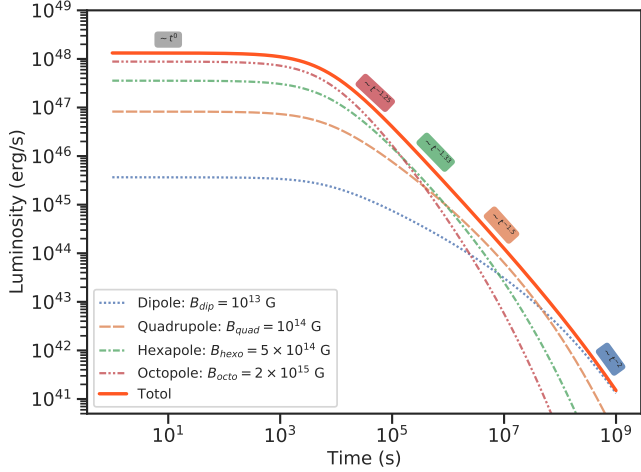


Figure 3. A magnetar having dipole, quadrupole, hexapole and octopole. The strength of magnetic field gets higher for the higher order multipole. Initially the high-order multipoles dominate the energy release, after 10^8 s (about three years), the dipole starts to be dominant.

creases over time, becoming negligible during the decay phase. The most significant difference from figure 1 is that, with all components present, the increase of spin period caused by the dipole leads to earlier arrivals and steeper decays of the decay phase for higher-order multipole components.

The third scenario also features the simultaneous presence of the dipole, quadrupole, hexapole, and octopole, but with magnetic field strengths increasing with the order. We chosen a dipolar field strength $B_{dip} = 10^{13}$ Gauss, a value weaker than the critical field. The strengths for the high-order multipolar components are as follows: quadrupole: $B_{quad} = 10^{14}$ Gauss, hexapole $B_{hexo} = 5 \times 10^{14}$ Gauss and octopole $B_{octo} = 2 \times 10^{15}$ Gauss. With such a configuration of magnetic fields, we obtain the figure 3. During the plateau phase of this scenario, the higher the order, the higher the spindown luminosity, this result differs from the previous scenarios. In the decay phase, as time progresses, the luminosity of the lower-order components gradually surpasses that of the higher order, and the decay index becomes

increasingly steep. Eventually, around 10^8 seconds later, the dipole dominates the spindown. Together with figure 2, we can conclude that under a reasonable magnetic fields configuration, regardless of the initial strength differences between the dipole and multipole components, the dipole component will eventually dominate the spindown. This means that from the observations of thousands of years after the birth of magnetar, regardless of whether the calculated dipole strength exceeds the critical field strength, we cannot exclude the possibility of the existence of multipoles exceeding the critical field strength. This inference aligns with our previous discussion on the observational examples.

4. PHENOMENA ASSOCIATED WITH BIRTH OF MAGNETAR

Magnetars can theoretically form from binary NS mergers and from single star collapse. The formation of magnetar is associated with and plays a critical role in various areas of astrophysics, including SLSN (Woosley 2010; Kasen & Bildsten 2010), GRBs (Piran 2004; Berger 2014) and FRBs (Petroff et al. 2022; Zhang 2023).

NS mergers (NS-NS) are expected to be important sources of gravitational waves (GWs; Abbott et al. 2017b; Belczynski et al. 2018; Abbott et al. 2023), with the outcome depending on factors such as the total mass of the NS-NS system and the equation of state governing NSs. These mergers can lead to the formation of a black hole (BH), the creation of temporary hyper-massive and supra-massive NSs, or a stable NS (Rezzolla et al. 2011; Rosswog et al. 2014; Ravi & Lasky 2014; Gao et al. 2016). For the single massive star, once the star depletes its nuclear fuel, the loss of pressure balance causes the core to collapse under its own gravity, then a NS or a magnetar could be born at the center (Bethe 1990; Mereghetti et al. 2015).

During the binary merger process and the single star collapse process, various mechanisms could amplify the magnetic field (Igoshev et al. 2021b). For example, the dynamo mechanism transforms kinetic energy into magnetic energy, that the rapid rotation and convective motions within the highly conductive neutron-rich matter can induce electric currents, which, in turn, are capable to generate magnetic fields of $\sim 10^{14} - 10^{15}$ Gauss (Duncan & Thompson 1992; Raynaud et al. 2020).

In the context of GRBs, long-duration GRBs (LGRBs) are often associated with type IC supernovae (Hjorth & Bloom 2012; Kovacevic et al. 2014; Cano et al. 2017; Aimuratov et al. 2023; Wang et al. 2019), leaving behind a newborn NS at the center of the explosion, while short-duration bursts (SGRBs) are hypothesized to originate from mergers of compact object binaries (NS-NS/BH mergers)(see e.g., Kumar & Zhang 2015; Zhang 2018, and references therein).

Approximately half of the LGRB light curves exhibit the “canonical” pattern, characterized by a sequence of steep, shallow (plateau), and normal decay phases (Nousek et al. 2006; Zhang et al. 2006). Moreover, a substantial majority of their X-ray emissions deviate from the expected single power-law decay predicted by the standard afterglow model (Meszaros & Rees 1993; Liang et al. 2009; Melandri et al. 2014; Bernardini 2015).

The presence of well-observed flaring activities alongside X-ray afterglow emissions suggests a significantly prolonged duration compared to their initial emission, typically extending up to around 100 seconds (Chincarini et al. 2010; Ruffini et al. 2018).

For SGRBs resulting from NS-NS mergers, observations with Swift have uncovered extended activity of the central engine, encompassing extended emission (EE), X-ray flares, and “internal plateaus” featuring rapid decay towards

the end of these plateaus (Norris & Bonnell 2006; Rowlinson et al. 2010; Lü et al. 2015). In fact, nearly half of short SGRBs exhibit a phase characterized by a prolonged plateau (D’Avanzo et al. 2014).

These observations pose challenges within the framework of a black hole central engine but are consistent with the concept of a rapidly spinning millisecond magnetar as the central engine (Metzger et al. 2008; Rowlinson et al. 2010). The magnetar central engine hypothesis offers a plausible explanation for the observed X-ray plateau during the GRB afterglow, as the magnetar is anticipated to dissipate its rotational energy (Usov 1992; Metzger et al. 2011; Zhang 2018; Wang et al. 2022, 2023).

Furthermore, the occurrence of “internal plateaus” in specific LGRBs and SGRBs has been identified as a compelling indicator of the presence of a millisecond magnetar in GRBs (Troja et al. 2007; Rowlinson et al. 2013; Tang et al. 2019; Du 2020; Li 2018).

Within the framework of the magnetar model, a feasible interpretation is that the NS is “supramassive” at birth and subsequently undergoes collapse to a black hole after significant spin-down, while this cannot be accounted for by an external shock model (Lü et al. 2015; Zhang 2018; Hou et al. 2021).

It should be noted that, prevailing in the above-mentioned works, following the classic formulation of Shapiro & Teukolsky (1983), (see also Gunn & Ostriker 1969; Michel 1982; Finn & Shapiro 1990), strong consideration has been given solely to the dipole component, with various higher order magnetic components being neglected.

4.1. *X-ray afterglow of GRBs observed by Swift*

Exploring the Swift database allows for the identification of additional GRBs exhibiting similar temporal characteristics, which could lead to a deeper understanding of the mecha-

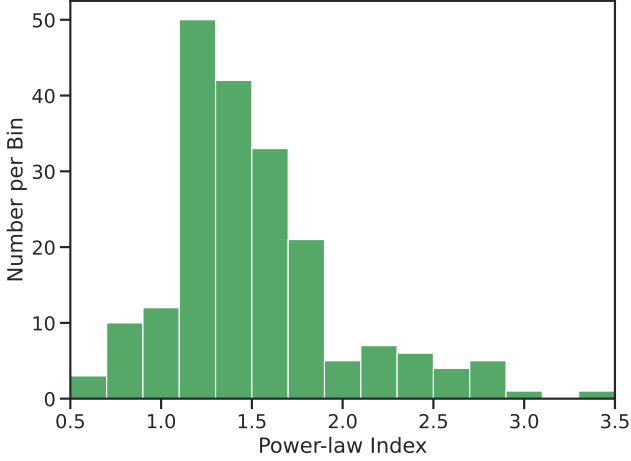


Figure 4. The histogram of power-law decay index of afterglow observed by Swift-XRT. In total 204 GRBs having a observed plateau structure till the end of March 2021. Most of the indices are between -1 and -2 , the median and mean value are -1.40 and -1.55 respectively (The index is defined as a negative value in this plot).

nisms driving these sources (see e.g., Nava et al. 2013; Dainotti et al. 2017; Rueda et al. 2020).

The UK Swift Science Data Centre², which provides ongoing updates to the dataset initially presented by Evans et al. (2009) offers a comprehensive database containing various properties of GRBs, such as their spectrum, position, light curve, and parameters derived from the best temporal power-law fits .

We explored the list and targeted the long or short GRBs whose afterglows exhibit a distinctive plateau phase followed by a temporal decay, described by a power-law function of the form $\propto t^\alpha$, where α represents the power-law index. Up to March 2021, we have identified a total of 204 GRBs exhibiting an observed plateau structure in their afterglows.

Figure 4 illustrates the distribution of power-law decay indices observed in the afterglows detected by Swift/XRT. The histogram indicates that the majority of the indices fall within the

² https://www.swift.ac.uk/xrt_products/index.php

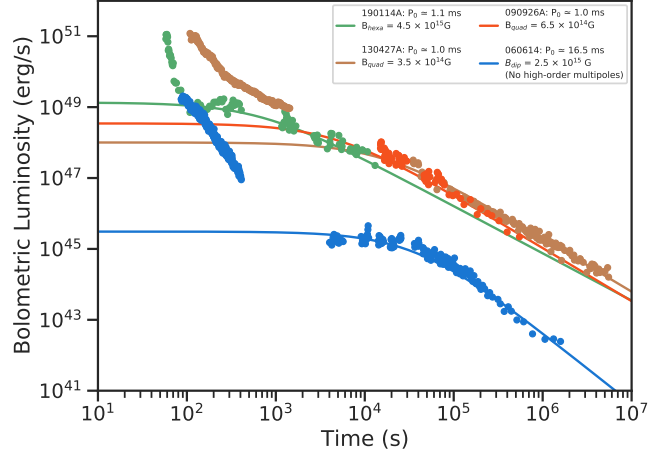


Figure 5. NS spin-down energy as the major energy source of the GRB outflow. The multipolar model surpasses the traditional dipole mode in fitting the normal decay, since the multipoles could inject energy (spin-down luminosity) following a wider range of power-law decay indices (-2 to -1). This figure shows some examples with fitted initial spin period (P_0) and the magnetic field components. The majority of GRB afterglows indicate the fast spinning newborn magnetars evolve high-order poles.

range of -1 to -2 , with median and mean values of -1.40 and -1.55 , respectively. This represents a common trend in the temporal decay behavior of these GRB afterglows, similar to the one predicted by higher orders of multipolar magnetic fields as discussed in the previous section. In the following section, we will investigate how this behavior can be effectively elucidated by the multipolar magnetic emissions.

5. FITTING GRB AFTERGLOW BY MAGNETAR MULTIPOLAR EMISSION

In the demonstration presented in section 3, it was highlighted that for magnetars with millisecond spins, the luminosity from multipole spindown can match or surpass that from dipole emission, and the lightcurve is composed of plateau followed by power-law decay, the decay index ranges between -1 and -2 . The discussion in section 4 explains that GRB can give birth to magnetar and shows consistent

pattern of plateau plus decay observed in the GRB afterglow, noting that the decay index of GRB afterglows again falls within the -1 to -2 range. Additionally, the light curve of CDF-S XT2 (Xue et al. 2019), the uniquely identified early-stage magnetar, exemplifies typical GRB afterglow features both temporally and energetically. In fact, CDF-S XT2 is believed to be the product of a binary NS merger. It probably has also produced a GRB, but the GRB is missed because the relativistic jet did not point to the satellites.

The above evidences prompt us to speculate that the plateau and subsequent normal decay phases of GRB afterglow are originated from the multipolar spindown energy of newborn magnetar.

We investigate this assumption for several GRBs of well observed X-ray afterglow data by Swift, including GRB 060614, GRB 090926A, GRB 130427A and GRB 190114A (Yang et al. 2015; Swenson et al. 2010; Ruffini et al. 2015; Xu & Tang 2021). We do not consider the radiation from the first few hundred seconds before the plateau, as this early radiation has different origins. We posit that the ratio of energy input from multipole to the observed energy in the afterglow is unity, due to the involvement of several uncertain parameters. Firstly, the radiation from the afterglow is beamed, but the angle of beaming cannot be precisely constrained. Ignoring the beaming effect leads to an increase in both the estimated spin period and the magnetic field strength (Rowlinson et al. 2010). These adjustments counterbalance the effect of not considering the conversion efficiency from rotational energy to radiative energy, which is also an uncertain value (Zhang et al. 2021; Li et al. 2023). This simplified treatment may bring an uncertainty of a factor of 3 (Rowlinson et al. 2013).

In figure 5, the observed luminosities of these GRBs afterglows are depicted, along with the

fitted curves by the multipolar emission. It can be seen that the model fits the observational data of the plateau and normal decay phases very well. The fittings reveal that GRB 090926A and GRB 130427A could be effectively modeled using a quadrupole emission, resulting in magnetar spins of 1 ms and magnetic field strengths of 6.5×10^{14} Gauss and 3.5×10^{14} Gauss, respectively. GRB 190114C aligns with hexapole emission, showing a spin of 1.1 ms and a magnetic field strength of 4.5×10^{15} Gauss. GRB 060614 fits a dipole model with a spin of 16.5 ms and a magnetic field strength of 2.5×10^{15} Gauss.

The spins of GRB 090926A, GRB 130427A, and GRB 190114A are all around 1 ms, which may be related to their afterglows being among the brightest in all observed GRBs. The light curve of GRB 060614 resembles that of the magnetar CDF-S XT2 (Xue et al. 2019). CDF-S XT2 is located at a redshift of $z=0.738$, on the outskirts of its host galaxy (Zheng et al. 2017). The light curve of CDF-S XT2 features a plateau of luminosity in the order of $10^{45} \text{erg s}^{-1}$ that persists for $\sim 2 \times 10^3$ s, succeeded by a sharp power-law decline of index $-2.16_{-0.29}^{+0.25}$ (Xue et al. 2019). GRB 060614 exhibits very similar luminosity strength and evolutionary behavior, except it has a longer duration of the plateau. The steep decay of the initial few hundred seconds observed in GRB 060614 but missed in CDF-S XT2 is reasonable, since in the case of CDF-S XT2, the jet which produces the initial steep decay is off-axis. GRB 060614 lacks the supernova association (Gal-Yam et al. 2006) but it is associated with a kilonova (Yang et al. 2015; Jin et al. 2016), suggesting it has the same origin as CDF-S XT2, that they are resulted from binary NS mergers.

Our fitting utilized a single dominant magnetic field component. In reality, other components might also be present. Due to the

precision of the data, we are unable to effectively constrain the parameters of these secondary components. However, we can attempt to limit the secondary components, ensuring that their maximal values do not introduce significant deviations to the fitting. For instance, for the quadrupole dominated GRB 130427A, there could also exist a dipole field with an upper limit of $\sim 6 \times 10^{13}$ Gauss and a hexapole field with an upper limit of $\sim 1.5 \times 10^{15}$ Gauss.

To conclude, the fitting parameters obtained for each GRB are consistent with the expected characteristics of newborn magnetars, lending support to the magnetar origin hypothesis for GRB afterglows. Furthermore, these results provide reciprocal support for the theories that GRBs can lead to the formation of magnetars.

6. DISCUSSION AND CONCLUSIONS

Our article is dedicated to investigating the multipolar radiation features of newly formed millisecond magnetars, specifically within the first year and even the first day following their birth. As highlighted in the Introduction, the role of multipolar emission is becoming increasingly prominent in explaining the properties of fast rotating NSs and the radiation in related phenomena, driven by advances in theoretical and computer simulations, as well as rapid growth in observations (Usov 1992; Zhang et al. 2005; Israel et al. 2017; Bilous et al. 2019; Philippov & Kramer 2022; Zhang 2023).

In Sections 2 and 3, we have presented a comprehensive analytical solution for the evolution of NS multipolar electromagnetic fields and their associated expected luminosities for a general magnetic field and mass of the NS. For simplicity, we have employed a simplified solution by treating the NS as a point-like source, rather than considering its finite size.

As an indicative application we have demonstrated that the emission from millisecond magnetars can serve as a source of GRB afterglow, explaining the occurrence of the GRB X-ray

plateau and its subsequent temporal decay with a power-law behavior. As shown in Section 4, the majority of the power-law decay indices observed in the afterglows of GRBs detected by Swift/XRT fall within the range of -1 to -2, with median and mean values of -1.40 and -1.55, respectively, which aligns well with the higher orders of multipolar emission from a millisecond magnetar.

The complex behavior observed in the afterglow emission of GRBs, which significantly deviates from the simple power-law decay predicted by the standard afterglow model (Meszaros & Rees 1993), has been elucidated. This highlights the potential of multipolar electromagnetic emissions from highly magnetized, rapidly rotating magnetars, in providing a more comprehensive understanding of the temporal characteristics of GRB afterglows and similar phenomena.

Our study is distinctive in that it diverges from the typical observation of approximately 1-second magnetars, in which the dipole component predominantly governs the spin down. Additionally, for a newly formed magnetar with a spin period of approximately 1 millisecond, the multipolar luminosity is comparable to the dipole and significantly contributes to the spin down and subsequent afterglow radiation of GRBs. The high luminosity from the multipole components, coupled with their flexible decaying behavior, allows us to effectively model various GRB afterglows, including the plateau and subsequent normal decay phases.

In principle, the prominence of higher orders of multipole radiation in highly rotating NSs, specifically those with periods $P \lesssim 1$ ms, introduces additional important considerations. In the case of slowly rotating NSs, the moment of inertia remains constant. However, for rapidly rotating NSs, their oblateness causes significant variations in its moment of inertia as the period

evolves, leading to notable observational implications (Shapiro & Teukolsky 1983).

For example, it has been demonstrated by Finn & Shapiro (1990) that during the initial stages of the evolution of a rapidly rotating star, the rotational frequency may increase even as the angular momentum decreases. This phenomenon is dependent on the specific nuclear equation of state adopted and could offer a potential explanation for the early flares superim-

posed on the afterglow emission observed in the X-rays of GRBs. However, a comprehensive investigation of this subject requires a separate study involving in-depth analytic and numerical treatments. Such an exploration could provide valuable insights into the underlying mechanisms driving the observed temporal behaviors in GRB afterglows and further enhance our understanding of the complex dynamics of highly rotating NSs.

REFERENCES

- Abbott, B. P., Abbott, R., Abbott, T. D., et al. 2017a, *ApJL*, 848, L13
- . 2017b, *ApJL*, 851, L16
- Abbott, R., Abbott, T. D., Acernese, F., et al. 2023, *Physical Review X*, 13, 011048
- Aimuratov, Y., Becerra, L. M., Bianco, C. L., et al. 2023, *ApJ*, 955, 93
- Alpar, M. A., Ertan, Ü., & Çalışkan, Ş. 2011, *ApJL*, 732, L4
- Barrera, R. G., Estevez, G. A., & Giraldo, J. 1985, *European Journal of Physics*, 6, 287
- Belczynski, K., Askar, A., Arca-Sedda, M., et al. 2018, *A&A*, 615, A91
- Berger, E. 2014, *ARA&A*, 52, 43
- Bernardini, M. G. 2015, *Journal of High Energy Astrophysics*, 7, 64, swift 10 Years of Discovery, a novel approach to Time Domain Astronomy. <https://www.sciencedirect.com/science/article/pii/S221440481500021X>
- Bethe, H. A. 1990, *Reviews of Modern Physics*, 62, 801
- Bilous, A. V., Watts, A. L., Harding, A. K., et al. 2019, *ApJL*, 887, L23
- Cano, Z., Wang, S.-Q., Dai, Z.-G., & Wu, X.-F. 2017, *Advances in Astronomy*, 2017, 8929054
- Chincarini, G., Mao, J., Margutti, R., et al. 2010, *Monthly Notices of the Royal Astronomical Society*, 406, 2113. <https://doi.org/10.1111/j.1365-2966.2010.17037.x>
- Dai, Z. G., & Lu, T. 1998, *A&A*, 333, L87
- Dainotti, M. G., Nagataki, S., Maeda, K., Postnikov, S., & Pian, E. 2017, *A&A*, 600, A98
- D’Avanzo, P., Salvaterra, R., Bernardini, M. G., et al. 2014, *Monthly Notices of the Royal Astronomical Society*, 442, 2342. <https://doi.org/10.1093/mnras/stu994>
- De Grandis, D., Taverna, R., Turolla, R., et al. 2021, *ApJ*, 914, 118
- de Lima, R. C. R., Coelho, J. G., Pereira, J. P., Rodrigues, C. V., & Rueda, J. A. 2020, *ApJ*, 889, 165
- Du, S. 2020, *ApJ*, 901, 75
- Duncan, R. C., & Thompson, C. 1992, *ApJL*, 392, L9
- Esposito, P., Rea, N., & Israel, G. L. 2021, in *Astrophysics and Space Science Library*, Vol. 461, *Timing Neutron Stars: Pulsations, Oscillations and Explosions*, ed. T. M. Belloni, M. Méndez, & C. Zhang, 97–142
- Evans, P. A., Beardmore, A. P., Page, K. L., et al. 2009, *MNRAS*, 397, 1177
- Finn, L. S., & Shapiro, S. L. 1990, *ApJ*, 359, 444
- Fiori, A., Razzano, M., Harding, A. K., et al. 2024, *arXiv e-prints*, arXiv:2403.07649
- Gal-Yam, A., Fox, D. B., Price, P. A., et al. 2006, *Nature*, 444, 1053
- Gao, H., Zhang, B., & Lü, H.-J. 2016, *PhRvD*, 93, 044065
- Geppert, U., Page, D., & Zannias, T. 1999, *A&A*, 345, 847
- Geppert, U., & Viganò, D. 2014, *MNRAS*, 444, 3198
- Gil, J., Melikidze, G., & Zhang, B. 2006, *ApJ*, 650, 1048
- Göğüş, E., Baring, M. G., Kouveliotou, C., et al. 2020, *ApJL*, 905, L31

- Gourgouliatos, K. N., & Hollerbach, R. 2018, *ApJ*, 852, 21
- Gourgouliatos, K. N., Wood, T. S., & Hollerbach, R. 2016, *Proceedings of the National Academy of Science*, 113, 3944
- Gunn, J. E., & Ostriker, J. P. 1969, *Nature*, 221, 454
- Hewish, A., Bell, S. J., Pilkington, J. D. H., Scott, P. F., & Collins, R. A. 1968, *Nature*, 217, 709
- Hjorth, J., & Bloom, J. S. 2012, in Chapter 9 in "Gamma-Ray Bursts, 169–190
- Hou, S.-J., Du, S., Liu, T., Mu, H.-J., & Xu, R.-X. 2021, *ApJ*, 922, 102
- Huang, L., & Yu, C. 2014, *ApJ*, 784, 168
- Igoshev, A. P., Hollerbach, R., Wood, T., & Gourgouliatos, K. N. 2021a, *Nature Astronomy*, 5, 145
- Igoshev, A. P., Popov, S. B., & Hollerbach, R. 2021b, *Universe*, 7, 351
- Israel, G. L., Belfiore, A., Stella, L., et al. 2017, *Science*, 355, 817
- Jackson, J. D. 1998, *Classical Electrodynamics*, 3rd Edition, 832
- Jin, Z.-P., Fan, Y.-Z., & Wei, D.-M. 2016, in *European Physical Journal Web of Conferences*, Vol. 109, *European Physical Journal Web of Conferences*, 08002
- Kalapothisarakos, C., Wadiasingh, Z., Harding, A. K., & Kazanas, D. 2021, *ApJ*, 907, 63
- Kasen, D., & Bildsten, L. 2010, *ApJ*, 717, 245
- Kaspi, V. M. 2010, *Proceedings of the National Academy of Science*, 107, 7147
- Kaspi, V. M., & Beloborodov, A. M. 2017, *ARA&A*, 55, 261
- Kirsten, F., Snelders, M. P., Jenkins, M., et al. 2021, *Nature Astronomy*, 5, 414
- Kovacevic, M., Izzo, L., Wang, Y., et al. 2014, *A&A*, 569, A108
- Kumar, P., & Zhang, B. 2015, *PhR*, 561, 1
- Kundt, W., & Schaaf, R. 1993, *Ap&SS*, 200, 251
- Lattimer, J. M., & Prakash, M. 2004, *Science*, 304, 536
- . 2007, *PhR*, 442, 109
- Li, A. 2018, in *Quarks and Compact Stars 2017 (QCS2017)*, 011025
- Li, L., Wu, X.-F., Lei, W.-H., et al. 2018, *ApJS*, 236, 26
- Li, L., Wang, Y., Ryde, F., et al. 2023, *ApJL*, 944, L57
- Liang, E.-W., Lü, H.-J., Hou, S.-J., Zhang, B.-B., & Zhang, B. 2009, *ApJ*, 707, 328
- Liang, E.-W., Zhang, B.-B., & Zhang, B. 2007, *ApJ*, 670, 565
- Lü, H.-J., Zhang, B., Lei, W.-H., Li, Y., & Lasky, P. D. 2015, *ApJ*, 805, 89
- Lyne, A. G., & Graham-Smith, F. 2005, *Pulsar Astronomy*
- Melandri, A., Covino, S., Rogantini, D., et al. 2014, *A&A*, 565, A72
- Mereghetti, S., Pons, J. A., & Melatos, A. 2015, *SSRv*, 191, 315
- Meszaros, P. 1992, *High-energy radiation from magnetized neutron stars*
- Meszaros, P., & Rees, M. J. 1993, *ApJ*, 405, 278
- Metzger, B. D., Giannios, D., Thompson, T. A., Bucciantini, N., & Quataert, E. 2011, *MNRAS*, 413, 2031
- Metzger, B. D., Quataert, E., & Thompson, T. A. 2008, *MNRAS*, 385, 1455
- Michel, F. C. 1982, *Reviews of Modern Physics*, 54, 1
- Mondal, T. 2021, *ApJL*, 913, L12
- Nava, L., Sironi, L., Ghisellini, G., Celotti, A., & Ghirlanda, G. 2013, *Monthly Notices of the Royal Astronomical Society*, 433, 2107. <https://doi.org/10.1093/mnras/stt872>
- Norris, J. P., & Bonnell, J. T. 2006, *ApJ*, 643, 266
- Nousek, J. A., Kouveliotou, C., Grupe, D., et al. 2006, *ApJ*, 642, 389
- Olausen, S. A., & Kaspi, V. M. 2014, *ApJS*, 212, 6
- Ostriker, J. P., & Gunn, J. E. 1969, *ApJ*, 157, 1395
- Papitto, A., Falanga, M., Hermsen, W., et al. 2020, *NewAR*, 91, 101544
- Petroff, E., Hessels, J. W. T., & Lorimer, D. R. 2022, *A&A Rv*, 30, 2
- Philippov, A., & Kramer, M. 2022, *ARA&A*, 60, 495
- Piran, T. 2004, *Reviews of Modern Physics*, 76, 1143
- Pétri, J. 2015, *Monthly Notices of the Royal Astronomical Society*, 450, 714
- Ravi, V., & Lasky, P. D. 2014, *MNRAS*, 441, 2433
- Raynaud, R., Guilet, J., Janka, H.-T., & Gastine, T. 2020, *Science Advances*, 6, eaay2732
- Rea, N., Viganò, D., Israel, G. L., Pons, J. A., & Torres, D. F. 2014, *ApJL*, 781, L17
- Rea, N., Esposito, P., Turolla, R., et al. 2010, *Science*, 330, 944

- Rea, N., Israel, G. L., Esposito, P., et al. 2012, *ApJ*, 754, 27
- Rea, N., Israel, G. L., Pons, J. A., et al. 2013, *ApJ*, 770, 65
- Rezzolla, L., Giacomazzo, B., Baiotti, L., et al. 2011, *ApJL*, 732, L6
- Riley, T. E., Watts, A. L., Bogdanov, S., et al. 2019, *ApJL*, 887, L21
- Rosswog, S., Korobkin, O., Arcones, A., Thielemann, F.-K., & Piran, T. 2014, *Monthly Notices of the Royal Astronomical Society*, 439, 744. <https://doi.org/10.1093/mnras/stt2502>
- Rowlinson, A., O'Brien, P. T., Metzger, B. D., Tanvir, N. R., & Levan, A. J. 2013, *MNRAS*, 430, 1061
- Rowlinson, A., O'Brien, P. T., Tanvir, N. R., et al. 2010, *MNRAS*, 409, 531
- Ruderman, M. A., & Sutherland, P. G. 1975, *ApJ*, 196, 51
- Rueda, J. A., Ruffini, R., Karlica, M., Moradi, R., & Wang, Y. 2020, *ApJ*, 893, 148
- Ruffini, R., Wang, Y., Enderli, M., et al. 2015, *ApJ*, 798, 10
- Ruffini, R., Wang, Y., Aimuratov, Y., et al. 2018, *ApJ*, 852, 53
- Scholz, P., Kaspi, V. M., & Cumming, A. 2014, *ApJ*, 786, 62
- Shapiro, S. L., & Teukolsky, S. A. 1983, *Black holes, white dwarfs and neutron stars. The physics of compact objects*, doi:10.1002/9783527617661
- Suvorov, A. G. 2023, *MNRAS*, 523, 4089
- Swenson, C. A., Maxham, A., Roming, P. W. A., et al. 2010, *ApJL*, 718, L14
- Tang, C.-H., Huang, Y.-F., Geng, J.-J., & Zhang, Z.-B. 2019, *ApJS*, 245, 1
- Taverna, R., & Turolla, R. 2024, *Galaxies*, 12, 6
- Thompson, C., & Duncan, R. C. 1993, *ApJ*, 408, 194
- Tiengo, A., Esposito, P., Mereghetti, S., et al. 2013, *Nature*, 500, 312
- Troja, E., Cusumano, G., O'Brien, P. T., et al. 2007, *ApJ*, 665, 599
- Turolla, R., & Esposito, P. 2013, *International Journal of Modern Physics D*, 22, 1330024
- Turolla, R., Zane, S., Pons, J. A., Esposito, P., & Rea, N. 2011, *ApJ*, 740, 105
- Turolla, R., Zane, S., & Watts, A. L. 2015, *Reports on Progress in Physics*, 78, 116901
- Usov, V. V. 1992, *Nature*, 357, 472
- Wang, W.-H., Xu, H., Wang, W.-Y., et al. 2021, *MNRAS*, 507, 2208
- Wang, Y., Becerra, L. M., Fryer, C. L., Rueda, J. A., & Ruffini, R. 2023, *ApJ*, 945, 95
- Wang, Y., Rueda, J. A., Ruffini, R., et al. 2019, *ApJ*, 874, 39
- . 2022, *ApJ*, 936, 190
- Woolsey, S. E. 2010, *ApJL*, 719, L204
- Xu, M., & Tang, Q. W. 2021, *ApJ*, 911, 76
- Xue, Y. Q., Zheng, X. C., Li, Y., et al. 2019, *Nature*, 568, 198
- Yang, B., Jin, Z.-P., Li, X., et al. 2015, *Nature Communications*, 6, 7323
- Zhang, B. 2018, *The Physics of Gamma-Ray Bursts*, doi:10.1017/9781139226530
- . 2023, *Reviews of Modern Physics*, 95, 035005
- Zhang, B., Fan, Y. Z., Dyks, J., et al. 2006, *ApJ*, 642, 354
- Zhang, B., & Mészáros, P. 2001, *ApJL*, 552, L35
- Zhang, B., Sanwal, D., & Pavlov, G. G. 2005, *ApJL*, 624, L109
- Zhang, B., Wang, Y., & Li, L. 2021, *ApJL*, 909, L3
- Zheng, X. C., Xue, Y. Q., Brandt, W. N., et al. 2017, *ApJ*, 849, 127